Computational and Structural Biotechnology Journal 19 (2021) 3372–3383

COMPUTATIONAL AND STRUCTURAL BIOTECHNOLOGY JOURNAL

journal homepage: www.elsevier.com/locate/csbj

Binding characteristics of staphylococcal protein A and streptococcal protein G for fragment crystallizable portion of human immunoglobulin G

Hae Gon Lee, Shinill Kang, Joon Sang Lee *

Department of Mechanical Engineering, Yonsei University, Seoul 03722, South Korea

ARTICLE INFO

Article history:
Received 3 February 2021
Received in revised form 29 May 2021
Accepted 30 May 2021
Available online 04 June 2021

Keywords:
Immunoglobulin G
Protein A
Protein G
Protein docking
Affinity chromatography
Molecular dynamics

ABSTRACT

In the wide array of physiological processes, protein–protein interactions and their binding are the most basal activities for achieving adequate biological metabolism. Among the studies on binding proteins, the examination of interactions between immunoglobulin G (IgG) and natural immunoglobulin-binding ligands, such as staphylococcal protein A (spA) and streptococcal protein G (spG), is essential in the development of pharmaceutical science, biotechnology, and affinity chromatography. The widespread utilization of IgG-spA/spG binding characteristics has allowed researchers to investigate these molecular interactions. However, the detailed binding strength of each ligand and the corresponding binding mechanisms have yet to be fully investigated. In this study, the authors analyzed the binding strengths of IgG–spA and IgG–spG complexes and identified the mechanisms enabling these bindings using molecular dynamics simulation, steered molecular dynamics, and advanced Poisson–Boltzmann Solver simulations. Based on the presented data, the binding strength of the spA ligand was found to significantly exceed that of the spG ligand. To find out which non-covalent interactions or amino acid sites have a dominant role in the tight binding of these ligands, further detailed analyses of electrostatic interactions, hydrophobic bonding, and binding free energies have been performed. In investigating their binding affinity, a relatively independent and different unbinding mechanism was found in each ligand. These distinctly different mechanisms were observed to be highly correlated to the protein secondary and tertiary structures of spA and spG ligands, as explicated from the perspective of hydrogen bonding.

1. Introduction

Biotechnology and biopharmaceutical researchers have devoted considerable resources to study the large-scale production of highly purified antibodies for a wide range of scientific applications [1,2]. To achieve this objective, various methods have been devised to enrich or purify the protein of interest from other proteins and macromolecules. Among the most powerful methods employed is affinity chromatography, also known as affinity purification. Through this method, the protein of interest is purified by virtue of its specific binding characteristics with immobilized ligands [3]. By stable covalent bonding, specific ligands are biochemically attached to an insoluble solid matrix, binding the biomolecules with a specific affinity to ligands when a complex mixture is introduced into the column [4,5].

In affinity chromatography processes, various binding ligands are commonly used depending on the target biomolecule. For example, substrate analogs, lectin, and avidin are utilized as ligands for purifying target proteins, such as enzymes, polysaccharides, and biotin [6,7]. Each affinity system requires its own set of sample preparation processes and has its advantages depending on the given research purpose. Among these, understanding the binding of immunoglobulin G (IgG), which is the most prevalent type of antibody in the blood, with natural immunoglobulin-binding ligands has been the focus of biochemical and biotechnology

Abbreviations: IgG, Immunoglobulin G; spA, Staphylococcal Protein A; spG, Streptococcal Protein G; MD, Molecular Dynamics; SMD, Steered Molecular Dynamics; APBS, Advanced Poisson–Boltzmann Solver; ELISA, Enzyme-linked Immunosorbent Assays; Fc, Fragment Crystallizable; RMSD, Root Mean Square Deviation; MM/PBSA, Molecular Mechanics Poisson–Boltzmann Surface Area; SASA, Solvent Accessible Surface Area; AFM, Atomic Force Microscopy; BIR, Between Protein–Protein Interface Residues.

* Corresponding author.
E-mail address: joonlee@yonsei.ac.kr (J.S. Lee).

https://doi.org/10.1016/j.csbj.2021.05.048

research [8]. This is because IgGs has been used as an essential constituent of therapeutic protein drugs for various diseases (e.g., cancer, inflammation, and infectious and autoimmune diseases) and as a basic component of various immunological assays, such as enzyme-linked immunosorbent assays (ELISA) and western blot analysis [9–13].

The wide utilization range of IgGs has allowed several research groups to devise methods for purifying or isolating the antibodies from complex mixtures. For the IgG type antibody purification, the chromatographies of staphylococcal protein A (spA) and streptococcal protein G (spG) have been the most popular choices as binding ligands to purify IgG [14–17]. The bacterial cell wall proteins spA and spG, which are generally purified from staphylococcus aureus and streptococci bacteria, respectively, are known to be reversibly bound to the fragment crystallizable (Fc) region of most mammalian immunoglobulins through strong binding mechanisms [18,19]. Through this reversible binding mechanism, the spA and spG chromatographs for IgG purification afford advantages over other ligands in terms of stability, target selectivity, and yield.

From a scientific perspective, the authors consider that two fundamental unknowns have to be resolved for future bioengineering designs and processes: (i) quantitatively identifying the tightness of the binding of IgG with the spA or spG ligand and (ii) exploring the underlying protein interactions enabling the binding. In biology, such inquisitiveness has aided in understanding the key aspects of various biological processes [20]. In addition, understanding the functions of these binding proteins may provide an important optimization protocol for formulating new drugs; it also affords insight into many essential elements of life. Hence, the exploration of the underlying interaction mechanism and mutual binding of IgG with spA or spG from the viewpoint of conformational and energetic change is extremely important.

Although some early studies have detected the presence of molecular interactions and provided information on the IgG–spA/spG binding characteristics, some straightforward details cannot be confirmed [21–24]. For example, the existence of molecular interactions and the nature of IgG binding with spA or spG can be detected using immunological assays (e.g., ELISA test). However, this method only provides relatively comparative data, not independent quantitative indexes, of the binding strengths of spA and spG with various mammalian immunoglobulins [25–27]. Similarly, other methods developed to date (for example, fluorescence spectroscopy, surface plasmon resonance spectroscopy, gel-shift assays, and equilibrium dialysis) are not only competitive binding analyses but also binary classification studies to predict whether the interaction between the receptor and the ligand exists [21,28–32]. These experiments alone do not provide a fundamental understanding of the factors that control the activity of biological systems.

These shortcomings of previous methods can be resolved by leveraging computational studies enabling the detailed investigation of mechanisms behind the reversible binding of receptor–ligand complexes in terms of ionic and hydrophobic interactions, hydrogen bonds, and van der Waals (vdW) forces [33,79]. However, there have been no in-depth studies on IgG-spA/spG complexes, even though they are the most prevalent combination in affinity chromatography. This is because most of the few direct and quantitative measurement studies on protein binding have been primarily focused on monomeric ligand complexes (e.g., linear short peptide with a small amount of residue rather than multimeric complexes) [33–37]. Moreover, the studies on larger ligands have been hampered by the inconvenience of modeling many rotatable bonds in flexible peptides and obtaining accurate high-resolution models of binding interfaces [38]. Nevertheless, these barriers have been overcome by recent advances in robust computational and experimental methods [38–40]. Accordingly, by employing these computational approaches, molecular dynamics (MD) simulations were performed to analyze the immunological response of the IgG Fc portion to the spA or spG ligand [41–43].

The objective of this study is to measure the binding strength of each complex and explicate the dominant factors between the IgG and spA/spG interactions; hence, some important characteristics of these reactions were thoroughly analyzed. First, the root mean square deviation (RMSD) was monitored to evaluate whether the crystalline structures of the proteins achieved the best-fit docking pose during their binding states. Second, a simulation of the steered molecular dynamics (SMD) protocol, which applied the pulling detachment force to analyze the binding strengths, was employed. The authors confirmed that the spA ligand was strongly bound to the IgG Fc portion than the spG ligand, and dissociation events occurred through a completely different mechanism due to differences in the secondary and tertiary backbone structures between spA and spG. Further, their different unbinding pathways and mechanisms were examined in terms of hydrogen bonding. Finally, to clarify the non-covalent interactions that mostly contributed to the binding reactions, various properties of each amino acid residue interactions, such as surface electrostatic map, hydrophobic bonding interactions, and binding free energy calculations, were evaluated. Although the contributions of non-covalent interactions were independently investigated, all of them corroborated the tight binding strength of the IgG-spA complex and the corresponding docking mechanism. The authors consider that these analyses allow the detailed exploration of the foregoing phenomena and are considerably useful for creating a strategy to develop new potent biotechnology designs and processes.

2. Materials and method

2.1. Binding complex preparation

The initial binding conformational structures were based on X-ray crystallographic data, including those on the IgG Fc portion and spA (PDB ID: 5U4Y) or spG (PDB ID: 1FCC) ligand obtained from the Protein Data Bank (PDB) [44,45]. Certain adjustments in each initial binding complex were applied before the simulations were conducted. The initial crystallographic complex models were modified by deleting the water molecules and co-crystallized ligands. Then, each refined binding complex structure of IgG–spA/spG was placed in a rectangular periodic boundary box and solvated with TIP3P water (solvent box size: $10.8 \times 10.8 \times 10.8$ nm^3) [46]. To neutralize the system, the counter ion pairs of K^+ and Cl^- were placed at random positions in the box using the Monte Carlo ion-placing method. The simulation models are shown in Fig. 1.

2.2. MD protocol for IgG–spA/spG equilibration

The MD simulations were performed using nanoscale molecular dynamics (NAMD) and large-scale atomic/molecular massively parallel simulator (LAMMPS) programs with the Chemistry at HARvard Macromolecular Mechanics (CHARMM) 36 force field [47–49]. A few simulation steps were performed before post-processing data were generated. First, each solvated IgG–spA/spG system was energetically minimized using the conjugate gradient method [50]. After minimization, the solvent was thermalized to 303.15 K and equilibrated for 1 ns under isothermal NVT ensemble conditions. Subsequently, a post-processing data production run was conducted for 50 ns under isothermal–isobaric NpT ensemble conditions at 101.325 kPa and 303.15 K to evaluate the dynamics of the complexes and check the stability of their crystal conformation. The atomic motion equations were integrated with a time step of

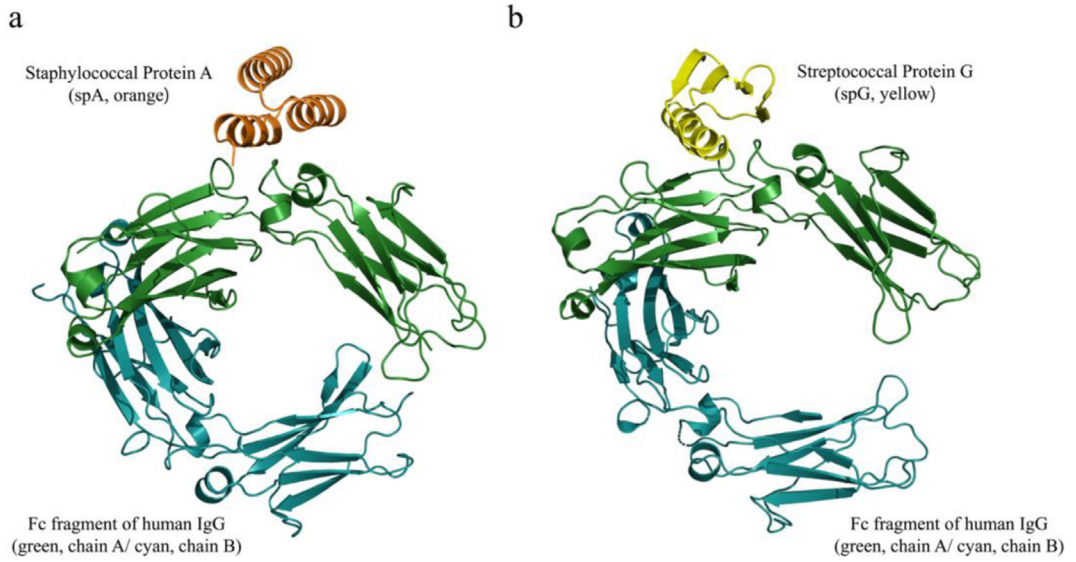

Fig. 1. Three-dimensional representation of protein crystalline structure between IgG Fc portion and proteins (a) A or (b) G; orange and yellow ribbons indicate spA and spG ligands, respectively. Two heavy chains in IgG Fc portion are marked with green and cyan ribbons. (For interpretation of the references to colour in this figure legend, the reader is referred to the web version of this article.)

2 fs, a cutoff distance of 12 Å for short-range interactions, and particle–particle particle–mesh solver for long-range interactions [51].

To constrain the covalent bonds of hydrogen atoms, the SHAKE algorithm was employed in the simulation [52,53], and a periodic boundary condition was applied to the *xyz*-directions. Configuration trajectories were collected every 10 ps for post-analysis, including hydrogen bonds, binding free energies, and RMSD calculations of the complexes. The formation of hydrogen bonds (H) was quantified via the Visual Molecular Dynamics Hbonds plugin when the distance between a hydrogen donor (D) and an acceptor atom (A) was less than 3.5 Å and angle D H···A was less than 60.0° [54]. The final configuration of each simulation was then employed as the initial configuration of the SMD calculations. The UCSF Chimera and Pymol software were used to obtain visual snapshots of each complex configuration, hydrogen bonding, electrostatic potential map, and hydrophobicity map [55,56].

2.3. SMD protocol for IgG–spA/spG unbinding

The SMD, an enhanced sampling MD approach, applies the harmonic potential to the atom or its aggregation to observe its response to external forces. This SMD approach provides insight into the binding strengths and ligand disassociation processes between binding receptors and ligands in response to mechanical forces [57,58]. In a typical SMD simulation, the complex of interest is pulled along a specific direction by applying a constant force or velocity on the atom or its aggregation [37,43,59]. Here, the constant pulling velocity approach was applied to the SMD simulation settings. The Cα atom of the 155th amino acid of spA (PRO_{155}) and the 1st amino acid of spG (THR_1) were attached to a harmonic virtual spring (Fig. S1). The virtual spring was moved with a constant velocity in the y direction perpendicular to the IgG-binding pocket. The force imposed on this spring is calculated using the following equations:

$$U_{harmonic} = \frac{1}{2}k_h(\vec{v} \times t - \vec{r})^2 \quad (1)$$

$$F_{harmonic} = -\nabla U_{harmonic} \quad (2)$$

where $U_{harmonic}$ is the potential energy; k_h represents the force constant of the harmonic potential function; $\vec{v}$ denotes the pulling velocity of a virtual atom; and t and $\vec{r}$ represent the simulation time and coordinate of the atom or atom aggregation with an additional action on itself, respectively. The measured force over time is recorded in a diagram form, demonstrating the force reaction of protein conformation states over time. For each complex, the results reported in this paper are based on the k_h and $\vec{v}$ values of 2.20 kcal/mol · Å^2 and 0.150 Å/ps, respectively. To prevent the freely dragged motion of the total complex by the external harmonic force imposed on spA/spG ligands, the Cα atoms of the 269th and 359th amino acid residues (GLU_{269}, THR_{359}) of both IgG proteins were fixed on the initial equilibrium positions (Fig. S1). To reduce the computational cost, the authors only considered directly docked heavy chains of the IgG Fc portion for the SMD simulations.

2.4. Free-binding energy calculation

The IgG–spA/spG free-binding energy or binding affinity were calculated using the molecular mechanics Poisson–Boltzmann surface area (MM/PBSA) method [60]. In the present study, MM/PBSA calculations were performed using the Calculation of Free Energy plugin powered by NAMD [47,54,61]. The calculated binding free energy values aid in determining the key amino acid sites from all the amino acid sequences by analyzing the binding energy contribution of each amino acid residue. For the MM/PBSA, three configuration trajectories (complex, separated receptor (IgG), and ligand (spA/spG)) should be extracted from the MD trajectory files. Then, the binding free energy (ΔG_{bind}) is obtained as the sum of different energy terms, as follows:

$$\Delta G_{bind} = \left\langle \Delta E_{gas} + \Delta G_{sol}^{polar} + \Delta G_{sol}^{nonpolar} - T\Delta S \right\rangle \quad (3)$$

The gas-phase free energy difference (ΔE_{gas}) between the complex and separate receptor or ligand (the first term on the right side of the equation) is obtained in the gas phase and can be divided into two components: vdW and electrostatic (ele) contributions, as follows:

$$\Delta E_{gas} = \Delta E_{vdW} + \Delta E_{ele} \quad (4)$$

Then, the polar solvation free energy difference (ΔG_{sol}^{polar}) is calculated using the advanced Poisson–Boltzmann solver (APBS) software [62]. The nonpolar solvation free energy difference is measured by estimating the approximate linear fitting relationship of the solvent-accessible surface area (SASA) difference. Subsequently, the change in the conformational entropy ($-T\Delta S$) is set equal to 0.0 in this study because the influence of this entropic term on a similar protein–protein binding complex is negligible [33,63]. Finally, the binding free energy, which has a less structural RMSD fluctuation, is summed and averaged over the selected trajectory periods.

3. Results and Discussions:

3.1. Secondary and tertiary structures of spA/spG

Before exploring the interactions of each IgG–spA/spG complex, fully comprehending the type of secondary structure composing the tertiary structure of spA or spG ligands is essential. Typically, alpha-helix and beta-sheet structures are the two most common types of protein secondary structures that are formed by hydrogen bonds between the carbonyl (*O*) of one amino acid and amino acid, *H*, of another. The alpha-helix segment is a rod-like structure in which tightly coiled main backbone chains form a right hand-helix conformation, and the beta-sheet segment is a planar structure composed of two or more segments of polypeptide chains (beta strands) that are laterally linked to each other, forming a sheet-like structure [64].

The configuration percentage of these two protein secondary structures performs a key role in protein function. Although spA and spG seem to have slightly similar structures, they yield different percentages of alpha-helix and beta-sheet structures, as shown in Fig. S2. The engineered IgG-binding domain of spA contains three alpha helixes in polypeptide segments from Lys_{105} to His_{116} (helix 1α), from Glu_{122} to Asp_{134} (helix 2α), and from Ser_{139} to Gln_{153} (helix 3α). The Ig-binding domains of spG is composed of a central alpha-helix segment encompassed by four beta strands: from ALA_{23} to ASN_{37} (helix 1β), from TYR_3 to GLY_9 (strand 1β), from LEU_{12} to THR_{18} (strand 2β), from GLU_{42} to THR_{44} (strand 3β), and from THR_{51} to THR_{55} (strand 4β).

Furthermore, understanding the role of hydrogen bonds in the formation of each protein's secondary structure is another requisite prior to exploring the binding characteristics. This concept is based on the fact that the formation mechanism is the reverse process of protein unbinding. The alpha-helix structure is only formed by the hydrogen bonds among amino acid residues in the same helix segment, whereas all hydrogen bonds are formed by different beta-strand segments in the beta-sheet structure. More intuitively, in the case of spA consisting of three alpha helixes, local and more frequently repeated hydrogen bonds are formed by four adjacent amino acid residues within the same helix structure with an axial distance of only 1.5 Å [64]. However, spG consisting of four mixed parallel/antiparallel beta strands with a single alpha-helix has less repetitive hydrogen bonds among the laterally aligned beta strands owing to the wide axial distances (3.5 Å) between adjacent amino acids [64]. Therefore, the spG polypeptide structures are generally more widely apart and form hydrogen bonds more subtly than those of spA. These different hydrogen bond formation processes in their secondary structures are linked to the peculiar binding properties of each complex in the subsequent section.

3.2. Stability analysis of IgG–spA and IgG–spG complexes

Before investigating the binding strength of each IgG–spA or IgG–spG, the RMSD values were calculated by measuring the difference between its initial backbone conformation and its next position. These values provide a specific and unified approach for analyzing and quantifying the stability of the proteins in the simulation: the lower the RMSD, the more stable the crystalline structure. To check the stability of each binding IgG–spA/spG complex, the RMSD values for the protein backbone are recorded during the 50-ns simulation, as shown in Fig. 2. For a simple and efficient calculation, only the RMSD of the protein backbone is considered by the authors; this technique is typically employed in many previous studies [34,65].

The RMSD values of each complex composed of the IgG Fc domain and spA or spG ligand are shown in Fig. 2 (a) and (b), respectively. Both complexes were observed as equilibrated during the simulation; however, fluctuations were visible. Both complexes were observed to equilibrate during the simulation; however, fluctuations were visible. The RMSD value is dependent on the molecular recognition state between the receptor and ligand, as well as the energetic interaction with the surrounding macromolecules; hence, this value is generally highly variable during the simulation. Moreover, both spA and spG ligands exhibited smaller structural fluctuations than the IgG Fc domain during each simulation, presenting average values of 1.00 ± 0.12 Å (spA) and 1.22 ± 0.22 Å (spG) versus 2.34 ± 0.49 Å (IgG Fc domain docked to spA) and 3.09 ± 0.61 Å (IgG Fc domain docked to spG), respectively. These time-averaged values are obtained over a simulation time of 50 ns. These results show each ligand is more stabilized than the IgG Fc domain.

Furthermore, to explore the structural stability and conformational changes within their binding interface more closely, the authors defined the protein–protein interface residues for each complex based on SASA calculations [66]. The protein–protein interface residues were predicted using a clustering algorithm to identify the surface regions with residues of high interface propensities [67]; the residues for each complex are listed in Table S1 and shown in Fig. S3. Various types of amino acid residues from both the IgG Fc portion and spA or spG ligand are included in the protein–protein interface residues. The RMSD values of these residues are shown in Fig. 2 (c) and (d). They are evidently more stabilized than each Fc region, presenting average values of 0.87 ± 0.17 Å (protein interface residues in IgG–spA complex) and 1.62 ± 0.32 Å (protein interface residues in IgG–spG complex). Although the protein–protein interface residues in the IgG–spA complex contain amino acid residues not only of spA but also the IgG Fc portion, they have a smaller and more stable RMSD value than all of the spA residues (1.00 ± 0.12 Å). Furthermore, the RMSD values that are less than 2.0 Å are known to be extremely meaningful for evaluating crystalline docking pose quality [35,63,68]. These results imply that the interface site of each complex considerably contributes to stability and tight binding.

To further analyze the role of protein–protein interface residues in their binding, the authors quantitatively tracked the number of hydrogen bonds formed between IgG and spA or spG and separated them into two categories: between protein–protein interface (BIR) and non-BIR residues (Fig. 3). Table S2 lists the details of the major residue pairs that form hydrogen bonds during the entire RMSD simulations; the list indicates that the amino acid pairs contribute to the binding stability. According to the data presented in Fig. 3, more than half of the hydrogen bonds, i.e., 72.3% and 89.3% for spA and spG, respectively, are derived from BIR interactions. Moreover, based on the summary in Table S2, the residues in helix 1α or 2α(for spA) and helix 1β (for spG) are majorly involved in forming the majority of stable hydrogen bonds than the other segments of each complex. The overall RMSD and hydrogen bonding results of each IgG–spA/spG complex intuitively indicate that the IgG Fc portion has maintained a stable binding state with spA/spG.

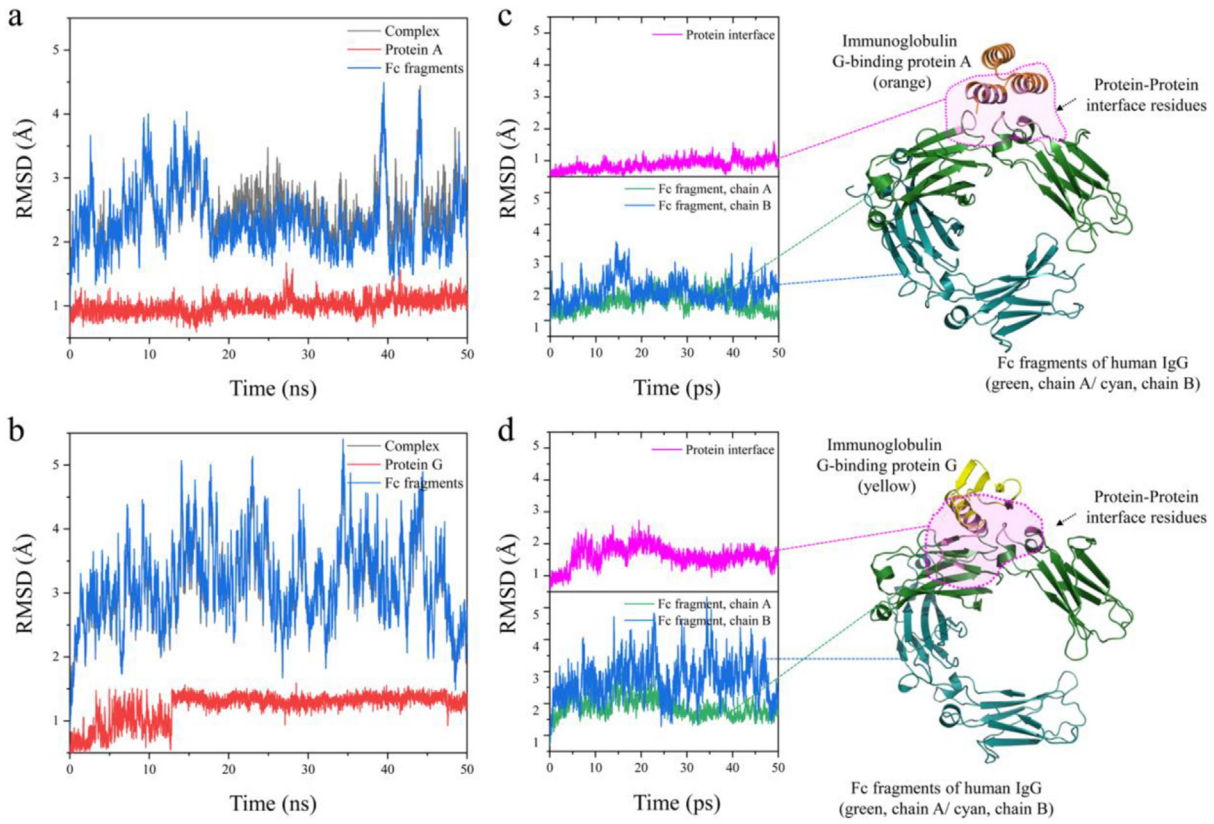

Fig. 2. RMSD of complexes calculated during 50 ns of MD simulations from initial conformations for (a) IgG–spA and (b) IgG–spG complexes; RMSD values of protein–protein interface residues and each heavy chain of IgG Fc domain are plotted in (c) and (d) with schematic of configuration pose of each complex on right.

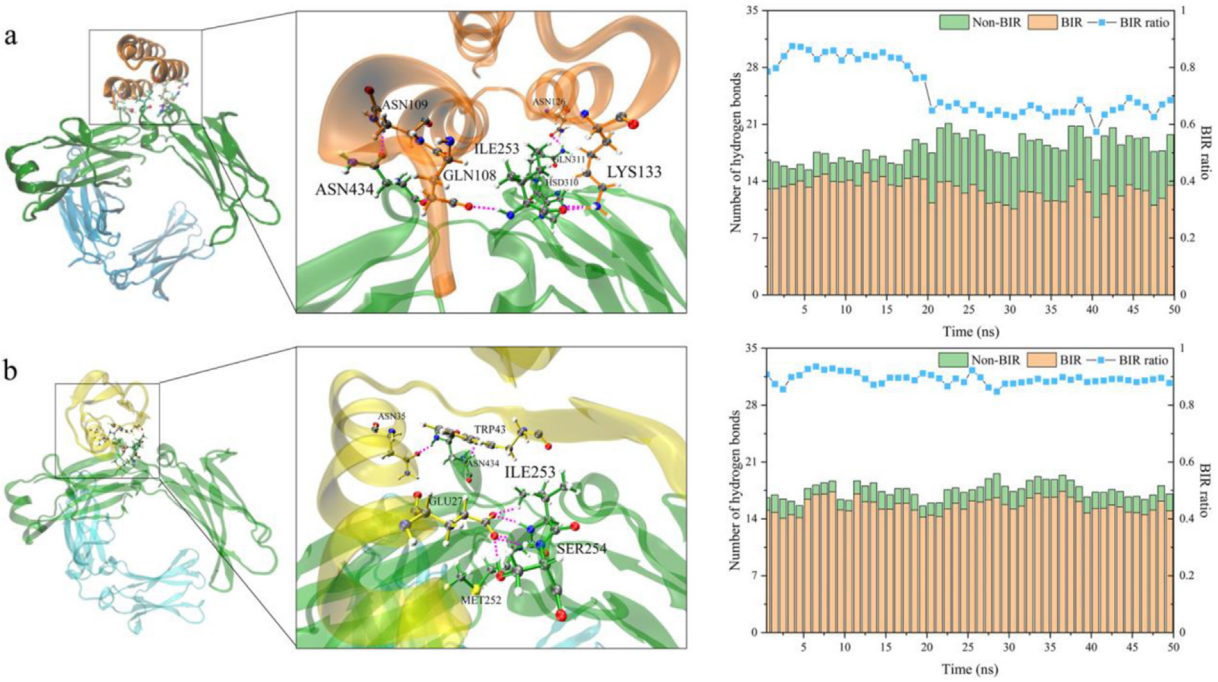

Fig. 3. Hydrogen bond contribution to stable crystalline binding structures: (Left) Highlighted key pair of hydrogen bonding residues; pink dotted line in middle inserts indicates key hydrogen bonds; (Right) number of hydrogen bonds formed between protein–protein interface residues (BIR) and non-BIR for (a) IgG–spA or (b) IgG–spG complex over time (BIR ratio obtained by dividing BIR hydrogen bond by total number of hydrogen bonds). (For interpretation of the references to colour in this figure legend, the reader is referred to the web version of this article.)

3.3. Binding strength and unbinding mechanism of IgG–spA/spG complexes

To calculate the binding strengths of each IgG–spA/spG complex, the authors replicated the experimental process of atomic force microscopy (AFM) via the SMD simulation that stretches and unfolds the secondary and tertiary structures of protein. The AFM protocol is a widely used experimental method that can provide information on the mechanical dissociation properties of the binding complex by applying an unbinding pulling force. The SMD is a long-established simulation technique that is known to well imitate the AFM protocol [37,42,59,69]. More importantly, the SMD methodology affords the opportunity to quantify the required binding strength for extracting spA or spG ligands from the IgG-binding pocket during the unbinding process. The evolution of the applied force during the SMD simulation considering the spA or spG ligand bound to the IgG Fc portion is shown in Fig. 4. The presented data confirmed that the different binding strengths and unbinding mechanisms depended on each binding ligand.

For an in-depth understanding of biomolecular processes, the authors endeavored to demonstrate the SMD results from the viewpoint of hydrogen bond formation and dissociation. The interpretation based on this perspective is based on two points. (i) During a stable binding state, the hydrogen bonds stabilize the protein secondary and tertiary structures; however, during unbinding, the converse occurs, breaking most hydrogen bonds; (ii) the spA and spG ligands have completely different protein structures except for one alpha-helix segment. The alpha-helix and beta-sheet structures are formed through different hydrogen bond formation processes (Section 3.1). With the foregoing considerations, the authors counted the number of hydrogen bonds formed between the inter-protein and intra-protein in the SMD simulations, as shown by the bottom panels in Fig. 4. Inter-protein hydrogen bonding is formed among different molecules (i.e., between the IgG Fc portion and spA or spG), whereas intra-protein hydrogen bonding exists within the molecule (i.e., within spA or spG ligand).

Based on the foregoing, the considerably different binding strengths and independent unbinding mechanisms of spA and spG with IgG could be explained. As shown in Fig. 4, the unbinding pathway consists of four sequence steps: complex maintenance process (yellow-shaded zone), alpha-helix unwinding or beta-sheet unfolding process (red-shaded zone), detachment process (blue-shaded zone), and protein unbinding process (green-shaded zone). The representative conformational changes during the unbinding process are shown by the top panels in Fig. 4; all inserted figures are enlarged in Fig. S4 with more detailed time steps. When Cα of the last amino acid residue (PRO_{155} for spA and THR_1 for spG) is first stretched using the SMD protocol, relatively monotonous force increments are observed on both complexes (yellow-shaded zones in Fig. 4(a) and (b)). For spA, this force increase is caused by the unbinding of helix 3α from the other alpha helixes and the pulled motion of helix 3α , as shown in Fig. S4 (a) at 150 ps. In addition, the total number of hydrogen bonds counted remains at approximately 88.1 with a small deviation. At approximately 152 ps, the force increase ceased; then, it decreased after reaching 674.4 nN, which is the required minimum force for spA to enter the next phase.

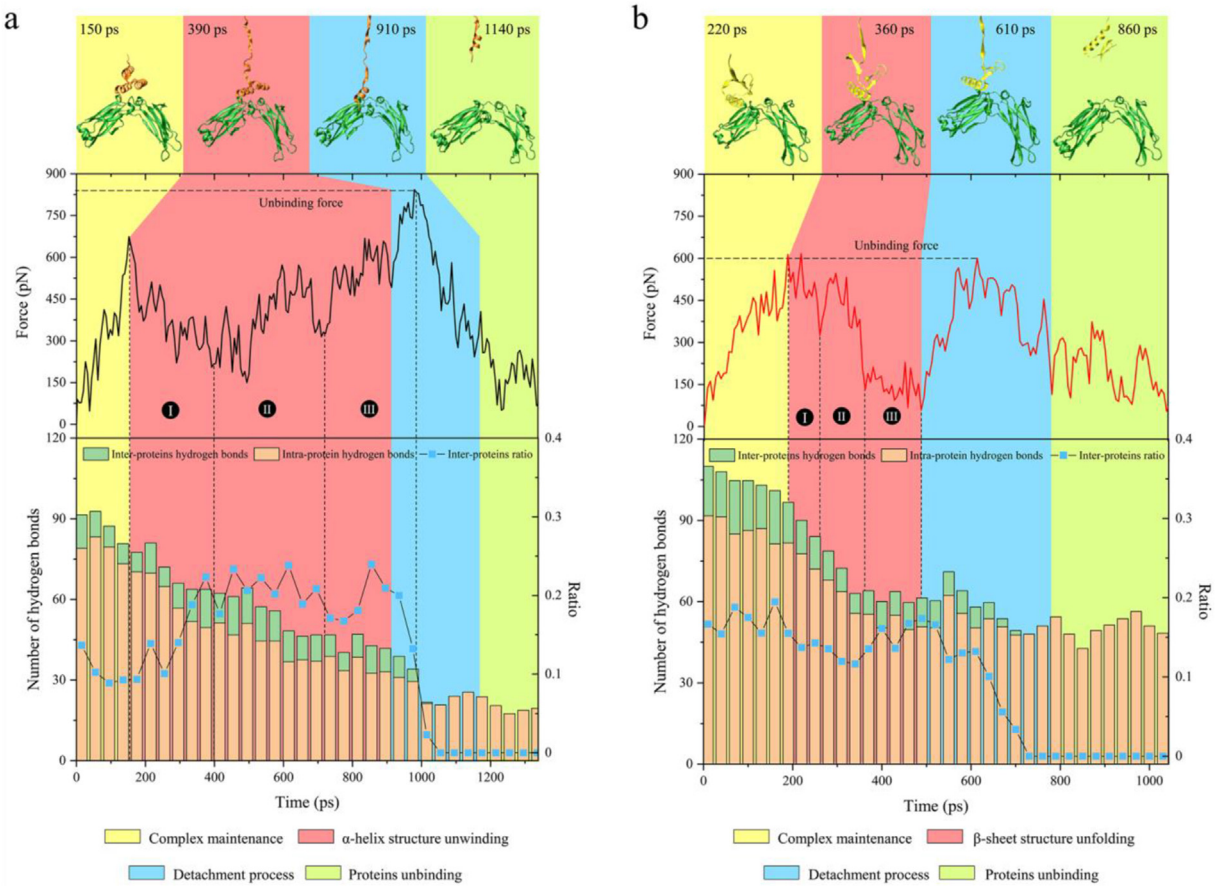

Fig. 4. Calculated forces over time to undock (a) spA ligand or (b) spG ligand from IgG binding site, and number of hydrogen bonds formed between inter-proteins and intra-protein for corresponding time. Inter-protein ratio is obtained by dividing the inter-protein hydrogen bond by total number of hydrogen bonds. Unbinding pathway consists of four sequence processes. For each process, representative conformations of each complex are shown in figure inserted above.

Thereafter, the force starts to decrease and considerably fluctuate, reaching an average of 421.7 nN (red-shaded zone). The highly variable forces are correlated to the unwinding behaviors of the 3α helix structure due to the pulling force. As mentioned, spA consists of three connected and aligned alpha helixes. Therefore, each alpha-helix is unwound in sequence and unbound from the IgG Fc portion when the external force is applied. The dotted lines in Fig. 4 indicate when each helix structure is unwound and unbound from the IgG binding pocket approximately from 152 to 392 ps (helix 3α), from 392 to 710 ps (helix 2α), and from 710 to 980 ps (helix 1α). The corresponding configurational change in the complex at each remarkable moment can be identified in Fig. S4(a).

For each of the three time domains, the inter-protein ratio fluctuates as much as the force curve. In the first time domain, the inter-protein ratio suddenly increases when the measured force resistance decreases. The reason for this is that the unwinding behavior of helix 3α particularly accelerates the breakdown of the intra-protein hydrogen bonds formed by every four adjacent amino acids in the same alpha-helix segment. However, the number of inter-protein hydrogen bonds does not significantly decrease because most of the stable inter-protein hydrogen bonds are majorly formed between IgG and helix 1α or 2α residues, as confirmed by the list in Table S2. Then, the pulling force starts to unwind helix 2α in the second time domain. In this domain, the inter-protein hydrogen bond ratio remains consistent with small deviations because as helix 2α unwinds, both inter-protein and intra-protein hydrogen bonds break at similar rates. This trend continues until 914 ps (end time of red-shaded zone) when the partial residues of helix 1α (from TYR_{112} to His_{116}) have been unwound. Thus, the measured force (i.e., 421.7 nN) primarily indicates the average force required to interrupt the intra-protein hydrogen bonds formed by every four adjacent amino acids in the same alpha-helix structure of the spA ligand.

Thereafter, the measured force spikes at approximately 914 ps (blue-shaded zone). The sharp peak is closely related to the behavior of helix 1α (particularly the specific amino acid residues from LYS_{105} to PHE_{111}). As shown in Fig. S4(a) at 910 and 980 ps, although the other residues in the same helix structure (from TYR_{112} to His_{116}) are smoothly unwound and undocked, the specific sequence of residues (from LYS_{105} to PHE_{111}) remains in their docking pose without unwinding until the applied force reaches the 843.1nN peak. However, when more force is applied, helix 1α detaches even without unwinding, as shown in Fig. S4(a) at 1140 ps. From the perspective of hydrogen bonding, the decoupling of spA with IgG occurs with the sudden breaking of all inter-protein hydrogen bonds; after the detachment process, the force gradually decreases (green shaded zone). Even after the dissociation, the amino acid residues (from LYS_{105} to PHE_{111}) retained the existing helical shape; hence, approximately 23.0 hydrogen bonds were maintained. The reason why these amino residues are not fully unwound is discussed in the next analysis section

For the IgG-spG case, the monotonous force raise is observed as seen with spA decoupling (yellow-shaded zone). However, in the case of spG, this increase is triggered by different reasons compared to the spA, considering that spG is composed of a central alpha-helix segment surrounded by four β-strands. When the pulling force is applied to Cα of the THR_1 residue in beta-strand 1β, the entire beta-sheet is detached from the central alpha-helix structure; the force reaches 613.9 nN at 188 ps. This configurational change is shown in Fig. S4(b) at 0 ps and 190 ps. The dissociation of the tertiary structure does not considerably influence the number of inter-protein and intra-protein hydrogen bonds because the protein tertiary structure is majorly formed and determined by the hydrophobicity of the side chain, rather than the hydrogen bonds. Amino acids with hydrophilic and hydrophobic side chains are usually found outside and inside the protein, respectively.

Subsequently, the force curve enters the red-shaded zone, where the beta-sheet structure is decomposed into three substates: approximately 188–260, 260–362, and 362–488 ps, as indicated by the dotted lines in Fig. 4(b). Two ridges and one plateau region were observed in the overall force decrease domain (188–488 ps). In the first ridge, beta strands 1β and 2β are isolated from other beta strands (4β and 3β) by the pulling force, as shown in Fig. S4(b) at 190 ps and 260 ps. The 616.7 nN peak is speculated to be the force required to break the intra-protein hydrogen bonds formed between strands 1β and 4β. Sequentially, beta strands 1β and 2β are unfolded into two parts at the second peak ridge value of 546.7 nN (Fig. S4(b) at 260 ps and 360 ps). Similarly, the intra-protein hydrogen bonds are steadily reduced in the second time domain due to the hydrogen bond interruption between strands 1β and 2β. For the third plateau domain (362–488 ps), the force and number of hydrogen bonds do not significantly change. This is related to the behavior when the already undocked but not fully unfolded beta strands (1β and 2β) are further stretched by the pulling force. The configurational changes are shown in Fig. S4(b) at 360 and 480 ps.

These results indicate that the force necessary to segregate strand 1β from 4β (617.7 nN) is higher than that necessary to separate it from strand 2β (546.7 nN). This is because a more stable hydrogen bond exists between the backbone and side chain of beta strands 1β and 4β. This is evinced by the fact that the average reduction in the number of intra-protein hydrogen bonds is higher in the first ridge domain (i.e., 20.0) than in the second domain (i.e., 15.0). In addition, the measured average force (i.e., 323.9 nN, red-shaded zone) during this β-sheet unfolding process is lower than the force required to unwind the alpha helixes in spA (i.e., 421.7 nN, red-shaded zone). This is because, as mentioned in section 3.1, the beta-sheet structure has fewer repeated hydrogen bonds than the alpha-helix structure. Such loosely bound hydrogen bonds cause resistance to the external force of the beta-sheet to be lower than the alpha helix. These results show that the unbinding pathway of each ligand is highly dependent on the protein secondary and tertiary structures of the ligand.

After beta-strand 1β is undocked and unfolded, the force considerably decreases to 58.8 nN and then starts to rebound (blue-shaded zone). This time domain (488–782 ps) in Fig. 4 is correlated to the unbinding processes of helix 1β, strand 3β, and strand 4β structures that are still attached to the IgG-binding pocket. The force curve suddenly increases and reaches 600.3 nN, which is the required force for segregating the spG ligand from IgG , as shown in Fig. S4(b) at 610 and 780 ps. The validity of this unbinding force value, compared to the experimental value, is described in the supplementary information section of S1. In monitoring the number of hydrogen bonds during the detachment process, all inter-protein hydrogen bonds are observed to break after the force reaches the peak values. This is because most stable inter-protein hydrogen bonds are mainly formed between IgG and the helix 1β residues, as summarized in Table S2. After the spG ligand is unbound, the force gradually decreases (green-shaded zone). Helix 1β and strands 3β and 4β retain the existing helical and beta-sheet conformation even after dissociation, respectively; hence, approximately 50.6 hydrogen bonds are maintained. This number is approximately twice that of the number of hydrogen bonds remaining after the spA ligand is undocked (23.0).

With respect to the binding strengths, the force for unbinding helix 1β (i.e., 600.3 nN) is lower compared with the force required to separate the helix 1α structure from IgG Fc portion (843.1 nN). This is unexpected given that practically the same alpha-helix segments of both ligands (helix 1α of spA or helix 1β of spG) are bound to similar IgG-binding sites immediately before the detachment process. Furthermore, the unwinding behaviors of the α-helix structure that can be distinctly observed in the unbinding

processes of helixes 2α and 3α in spA are virtually not observed in the unbinding process of helix 1β although they have similar secondary protein structures. The unwinding behavior only occurs in the few amino acids, from ALA_{23} to THR_{25} in helix 1β. This is practically the same peculiar phenomenon that has been observed in the unwinding behavior of the helix 1α segment in the spA ligand; the specific sequence of residues (from LYS_{105} to PHE_{111} in helix 1α and from GLU_{26} to ASN_{37} in helix 1β) is undocked without the unwinding behavior. To explain the foregoing phenomenon, the following analysis section discusses the underlying mechanisms involved.

3.4. Non-covalent interactions of protein–protein interface residues in IgG–spA/spG complexes

To further explicate the considerable binding strength of the IgG–spA complex compared with that of IgG–spG and the similar peculiar unbinding conformation of the helix segment, which is undocked without unwinding, the authors performed calculations for three types of protein interactions. Among the various components of molecular energetics, understanding the electrostatic interactions, hydrophobic bonding, and binding free energies among proteins is particularly important in examining the binding complex of interest. Because the protein binding reaction is a combinational consequence of these non-covalent interactions at specific binding domains on each protein, these examinations let us thoroughly comprehend how such a binding strength and unbinding mechanisms are observed for each IgG-spA/spG complex.

First of all, the authors considered that the analyses, in the perspective of the electrostatic and hydrophobic bonding features at the binding site, could explain why the alpha-helix structure in spA has more resistance to be undocked from IgG than that in spG. The electrostatic potential and hydrophobicity maps were obtained using APBS and UCSF Chimera tools [55,62,70]. The charge distribution maps for both complexes, separated receptors, and ligands are plotted in Fig. 5. These maps are useful for evaluating the role of electrostatic repulsion and attraction in binding complex formation and maintaining. These charge values decal into a protein surface representation map. The detailed configuration pose that is obscured in these charge distribution maps can be confirmed by the transparent surface maps shown in Fig. S5. The results indicated that the side portion of helixes 2α and 3α in spA (belonging to the protein–protein interface residues) were positively charged, and a relatively negatively charged binding pocket was formed on the Fc portion of IgG. However, for the IgG–spG complex, whereas the interface residue surface on the IgG Fc portion still had negative electrostatic values, a relatively neutrally charged binding pocket was observed in the interface of spG ligand residues.

In addition, the hydrophobicity maps are plotted in Fig. 6. These hydrophobic domains could be small binding clefts with only a few peptides or large surfaces with hundreds of polypeptide segments. It is well known that the binding strength or affinity is largely influenced by the size of the hydrophobic domains [71]. This is because the hydrophobic bonds allow the nonpolar surface residues to expel the water molecules between them, thus minimizing the water contact area and allowing the residues to aggregate tightly [72]. The opaque regions in Fig. 6 indicate the location of the surface of protein–protein interface residues and its contribution to the formation of a hydrophobic surface on each protein surface. Fig. S6 shows how the opaque regions of the protein–protein interfaces are actually identified in each docking structure. The interfacial residue surface in each protein can be further divided into a few regions depending on the hydrophobicity. These are α, β, γ/α', β', and γ' for the IgG–spA complex or α, β/α', and β' for the IgG–spG complex, where the α, β, and γ regions face the α', β', and γ' regions upon binding, respectively. To understand the hydrophobic interactions, the focus should be on the hydrophobic regions (i.e., β and β' for each IgG–spA/spG complex).

For the IgG–spA complex, a strong and wide area of hydrophobic surface, i.e., the β region (including ALA_{110}, PHE_{111}, ILE_{114}, LEU_{115}, and ILE_{129} residues) in the spA ligand, was observed as hydrophobically interacting with the β' region (e.g., PRO_{247}, LEU_{251}, MET_{252}, ILE_{253}, and LEU_{314} residues) in the IgG Fc portion (Fig. 6). However, in the case of spG, the interface surface has hydrophilic surfaces with only two hydrophobic amino acid residues, i.e., ALA_{23} and ALA_{24}. Therefore, the presented data show that weak and confined hydrophobic bonding occurs between the hydrophobic β region in the spG ligand and β'region (e.g., PRO_{247},

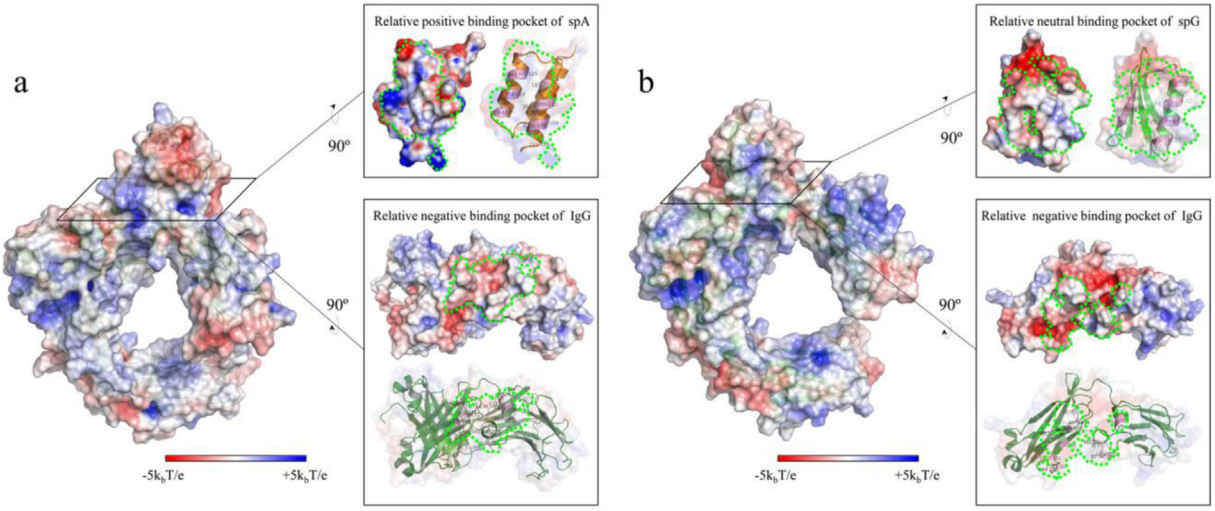

Fig. 5. Electrostatic potential maps of (a) IgG–spA and (b) IgG–spG complexes where interaction site is expressed on horizontal plane. Blue area has high potential with relatively no electrons (positive charge). Red area has low potential and relatively abundant electrons (negative charge). White area between red and blue has neutral charge. Right rotational inserts show electrostatic interaction of complexes on each ligand or receptor binding pocket. Green dotted line on electrostatic surface show location of protein–protein interface residues. Detailed configuration poses of each protein are represented by transparent surface maps. (For interpretation of the references to colour in this figure legend, the reader is referred to the web version of this article.)

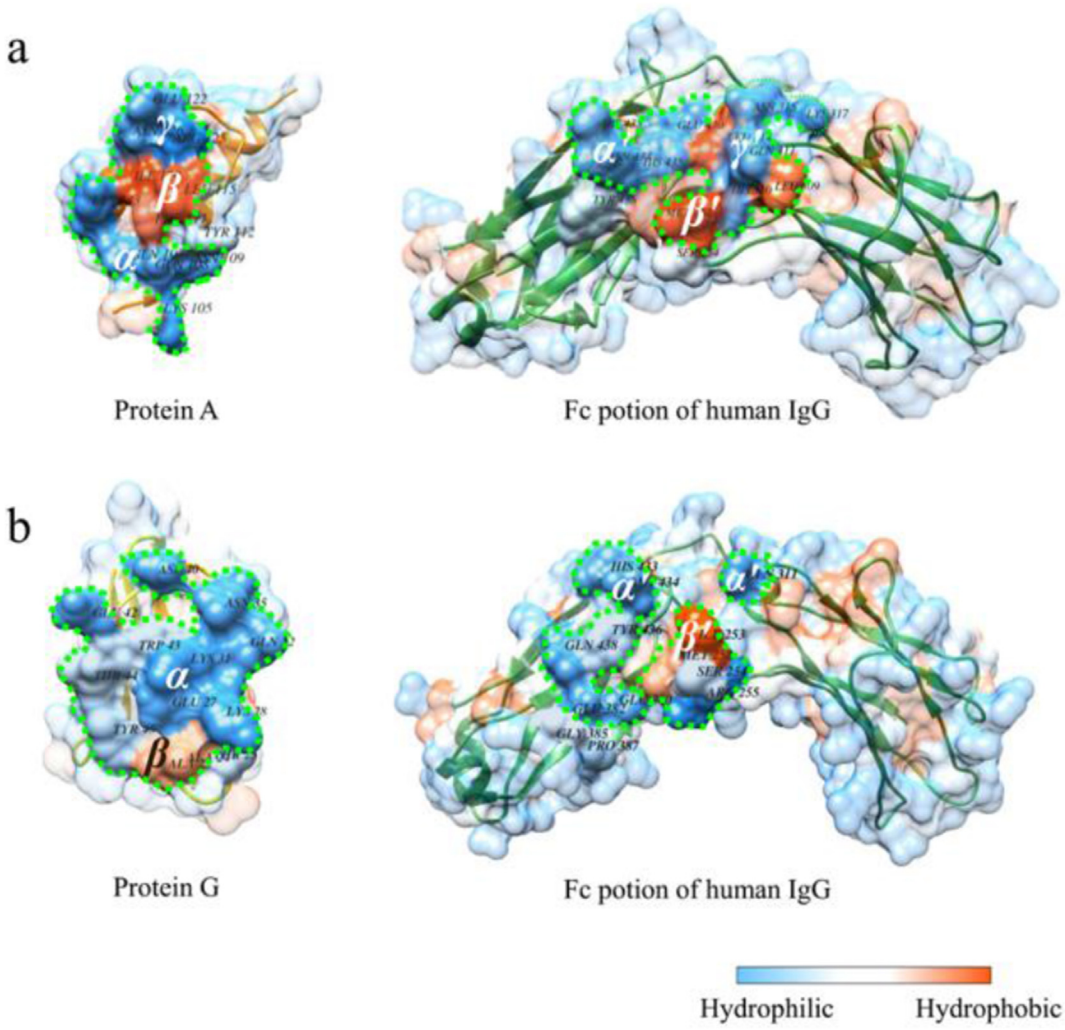

Fig. 6. Mapping hydrophobicity of each protein surface. Surface hydrophobicity map of protein–protein interface residues is opaque and surrounded by green dotted line. Orange and blue portions denote the most hydrophobic and hydrophilic areas, respectively. (For interpretation of the references to colour in this figure legend, the reader is referred to the web version of this article.)

LEU_{251}, MET_{252}, and ILE_{253} residues) in the IgG Fc portion. Based on the information derived from these non-covalent interaction analyses, the higher binding affinity in the α-helix structure in spA than that in spG can be explained, i.e., a strong electrostatic and hydrophobic attraction is present in the protein–protein interface residues of the IgG–spA complex.

Furthermore, there is still one remaining question: why was the specific sequence of amino-acid residues (from LYS105 to PHE111 in helix 1α, GLU26 to ASN37 in helix 1β) not unwound and directly detached? To answer this, the authors calculated the binding free energy contributions of each protein–protein interface residue in both the spA and spG ligands, as listed in Table S1. The binding free energy (ΔG_{bind}) calculations were performed for 5 ns (corresponding to 500 frames), extracted from the equilibrium phase of the RMSD simulation (25–30 ns). The higher the negative ΔG_{bind} value of each amino acid, the more that each amino acid contributes to the stable docking with the IgG Fc portion. This is because the molecular structures generally tend to stabilize toward the lowest energy configuration.

Therefore, the results shown in Fig. 7(a) intuitively suggest that most protein–protein interface residues in the spA ligand (GLN_{107}, GLN_{108}, ASN_{109}, PHE_{111}, TYR_{112}, LEU_{115}, ARG_{125}, ASN_{126}, and ILE_{129}) are involved in the tight binding with the IgG Fc portion. Among all the protein–protein interface residues, we were interested in the residues in the helix 1α segment, which was involved in the peculiar unbinding conformation. Except for the LYS_{105} residue, all of the helix 1α residues have negative binding free energy. In particular, from the perspective of energy decomposition, the amino acid of PHE_{111} contributes to the most stable energetic interaction among all the interface residues. Furthermore, the amino acid of PHE_{111} is confirmed to be involved in the hydrophobic bonding formation, as shown in Fig. 6. This hydrophobic bonding provides an energetically favorable binding site for the spA ligand. The high energetic stability and hydrophobic interaction between the PHE111 and the IgG Fc portion prevented the pulling force from propagating to the amino-acid sequence below; consequently, the specific sequence of the helix 1α structure (LYS105 to PHE111) was not fully unwound, but directly undocked.

However, for the spG ligand, a different mechanism led to these peculiar unbinding phenomena and weak binding strengths. In contrast to the spA ligand, a strong positive binding free energy is observed in the amino acid sequence from GLU_{27} to GLN_{32} in helix 1β (Fig. 7b); this suggests that these residues do not actively interact with the IgG-binding active site. Therefore, after the pulling force unwinds the small portion of helix 1β (from ALA_{23} to THR_{25}), the above amino acid sequence in the helix 1β segment (from GLU_{26} to ASN_{37}) easily undocks from the binding pocket without significant resistance. In particular, the calculated binding

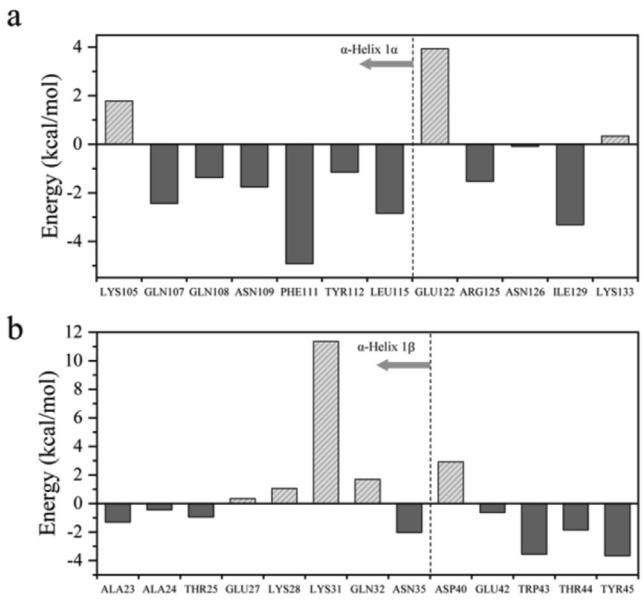

Fig. 7. Binding free energy of protein–protein interface residues in (a) spA and (b) spG ligands. Gray arrows indicate protein secondary segment to which residue belongs. Helix 1α or 1β structure is segment of interest in which peculiar unbinding conformation is observed.

free energy of LYS_{31} indicates that this residue is a key amino acid responsible for the binding strength of the spG ligand being lower than that of the spA ligand.; this residue does not contribute to the binding of spG to the IgG Fc portion. Although the non-covalent interactions were independently investigated, the investigation results collaboratively explained the high binding strength of the IgG–spA complex and the corresponding peculiar docking mechanism.

4. Conclusion

Understanding the underlying details of the binding characteristics between the IgG Fc portion and natural IgG-binding ligands (e.g., spA or spG) is of primary interest in devising many immunoassays and chromatography applications. Furthermore, this progress may have significant biotechnical implications for researchers to understand the role of each protein's secondary structure on the docking mechanisms. This is because each of the ligands is primarily composed of different major protein secondary structures except for one alpha-helix segment (e.g., three alpha helixes for spA or four beta strands with one alpha-helix for spG). This study involved an in-depth computational investigation to ascertain the binding strengths of each ligand and to determine which non-covalent interactions or amino-acid sites play a pivotal role in their tight binding. The stabilities of docked crystallographic complexes were evaluated through RMSD calculations during the 50-ns simulation. In particular, the RMSD values and number of hydrogen bonds of protein–protein interface residues show that the highly stable and tight docking states are attributable to their interface residues.

Based on these binding conformations, the distinct variation force curves of each complex were observed using the SMD protocol, which employs the pulling detachment force to investigate the binding affinity. According to the presented data, relatively different spA/spG binding strengths and independent unbinding mechanisms with IgG are observed. In addition, the binding strengths and unbinding mechanisms, which could be explained in terms of hydrogen bonding, are confirmed to be primarily correlated to the protein secondary and tertiary structures of spA and spG. The higher average unwinding force of the helix segment in spA (421.7 nN) compared with the unfolding force of the sheet segment in spG (323.9 nN) can be attributed to the more repeated intra-protein hydrogen bonds in the alpha-helix segment than in the beta-sheet structure. Although seemingly similar force curve patterns are observed in both complexes, each unbinding mechanism occurs with a different sequence of dissociation processes. This is proven by the results of tracking the number of inter-protein or intra-protein hydrogen bonds. However, there remain two unresolved questions: (i) Despite the fact that they were similarly docked, a far stronger force was needed to undock the spA ligand (843.1 nN) from the IgG Fc portion than spG (600.3 nN). (ii) The specific sequences of residues (from LYS_{105} to PHE_{111} in helix 1α and from GLU_{26} to ASN_{37} in helix 1β) were not fully unwound but were directly undocked by the pulling force, in contrast to the other helix residues.

The detailed analyses of the non-covalent interactions (e.g., electrostatic interactions, hydrophobic bonding, and binding free energies between the proteins) allowed us to resolve the aforementioned questions. These collaborative energetic analyses from the perspective of electrostatic and hydrophobic bonding features explain why the alpha-helix structure in spA experiences more resistance than the spG to be undocked from IgG. The results obtained from this computational study indicate that a more distinct oppositely charged and broad hydrophobic surface is observed at the interface of the IgG–spA complex consisting of protein–protein interfacial residues. This finding shows the electrostatic and hydrophobic contributions to the specificity and affinity of each ligand. The binding free energy calculations prove that the presence of key amino acids on each ligand (PHE_{111} in spA or LYS_{31} in spG) is involved in the peculiar undocking conformation and binding strength. In addition, in both complexes, not fully unwound configurations of alpha-helix segments were observed; however, the mechanisms behind these phenomena were confirmed to be different. This is because the key amino acids of each ligand oppositely affected their unwinding behaviors.

The authors believe that the results of this study have three representative implications in biotechnology. First, these intuitive and quantitative observations can be useful for biochemists and biophysicists to decide the bacterial protein to use in experiments such as immunoprecipitation techniques, double sandwich immunoassays, and affinity purification [73,74]. Conventionally, the experimenter knew from experience whether spA binds to human IgGs more strongly than spG but did not know how strongly they bind and what non-covalent intermolecular interactions facilitate this [73,75,76]. Thus, the results presented may rectify this ambiguous situation for biochemists and biophysicists. Second, the development of synthetic bacterial proteins to isolate human IgGs would be necessary for the sustainable and reliable production of these antibodies in the near future [18,77]. This knowledge will be of considerable use to the advancement of the future artificial protein industry by identifying the amino acid types and protein-coding sequence optimization that are important in terms of improving the binding capacity of synthetic proteins [78]. Third, these simulation results can bridge the apparent gap between direct observations through experiments and the actual events occurring in such a short nano-time scale. Using these intuitive results of our simulation, it is possible to infer the events that occurred by simply analyzing the AFM force curves without directly observing them in experiments.

CRediT authorship contribution statement

Hae Gon Lee: Conceptualization, Methodology, Software, Writing - original draft. **Shinill Kang:** Writing - review & editing,

Supervision. **Joon Sang Lee:** Writing - review & editing, Supervision, Project administration, Funding acquisition.

Declaration of Competing Interest

The authors declare that they have no known competing financial interests or personal relationships that could have appeared to influence the work reported in this paper.

Acknowledgments

This work was supported by a National Research Foundation of Korea (NRF) grant funded by the Korean Government (MSIP) (No. 2015R1A5A1037668).

Appendix A. Supplementary data

Supplementary data to this article can be found online at https://doi.org/10.1016/j.csbj.2021.05.048.

References

[1] Leavy O. Therapeutic antibodies: past, present and future. Nat Rev Immunol 2010;10(5):297.
[2] Matera MG et al. Therapeutic Monoclonal Antibodies for the Treatment of Chronic Obstructive Pulmonary Disease. Drugs 2016;76(13):1257–70.
[3] Lowe, C.C.R. and P.P.D. Dean, Affinity chromatography. 1974: John Wiley & Sons.
[4] Bailon, P., Affinity chromatography: methods and protocols: Springer Science & Business Media; Vol. 421. 2008
[5] Bonner, P., Protein purification; 2018: Taylor & Francis.
[6] Kumar, P., Fundamentals and Techniques of Biophysics and Molecular biology. 2018: Pathfinder Publication unit of PAPL.
[7] Rarbach M et al. Dual-color fluorescence cross-correlation spectroscopy for monitoring the kinetics of enzyme-catalyzed reactions. Methods 2001;24 (2):104–16.
[8] Merchant AM et al. An efficient route to human bispecific IgG. Nat Biotechnol 1998;16(7):677–81.
[9] Carter PJ. Introduction to current and future protein therapeutics: A protein engineering perspective. Exp Cell Res 2011;317(9):1261–9.
[10] Casadevall A, Dadachova E, Pirofski L. Passive antibody therapy for infectious diseases. Nat Rev Microbiol 2004;2(9):695–703.
[11] Dimitrov DS. Therapeutic antibodies, vaccines and antibodyomes. Mabs 2010;2(3):347–56.
[12] Kuno G, Gomez I, Gubler DJ. An Elisa Procedure for the Diagnosis of Dengue Infections. J Virol Methods 1991;33(1–2):101–13.
[13] Choe W, Durgannavar TA, Chung SJ. Fc-Binding Ligands of Immunoglobulin G: An Overview of High Affinity Proteins and Peptides. Materials 2016;9(12).
[14] Hjelm H, Hjelm K, Sjoquist J. Protein A from Staphylococcus aureus. Its isolation by affinity chromatography and its use as an immunosorbent for isolation of immunoglobulins. FEBS Lett 1972;28(1):73–6.
[15] Hober S, Nord K, Linhult M. Protein A chromatography for antibody purification. J Chromat B-Anal Technol Biomed Life Sci 2007;848(1):40–7.
[16] Moks T et al. Staphylococcal protein A consists of five IgG-binding domains. Eur J Biochem 1986;156(3):637–43.
[17] Björck L, Kronvall G. Purification and some properties of streptococcal protein G, a novel IgG-binding reagent. J Immunol 1984;133(2):969–74.
[18] Nilsson B et al. A Synthetic Igg-Binding Domain Based on Staphylococcal Protein-A. Protein Eng 1987;1(2):107–13.
[19] Guss B et al. Structure of the Igg-Binding Regions of Streptococcal Protein-G. EMBO J 1986;5(7):1567–75.
[20] Rizo J, Rosen MK, Gardner KH. Enlightening molecular mechanisms through study of protein interactions. J Mol Cell Biol 2012;4(5):270–83.
[21] Saha K, Bender F, Gizeli E. Comparative study of IgG binding to proteins G and A: nonequilibrium kinetic and binding constant determination with the acoustic waveguide device. Anal Chem 2003;75(4):835–42.
[22] Peng Z, Simons FER, Becker AB. Differential Binding-Properties of Protein-a and Protein-G for Dog Immunoglobulins. J Immunol Methods 1991;145(1–2):255–8.
[23] Lund LN et al. Exploring variation in binding of Protein A and Protein G to immunoglobulin type G by isothermal titration calorimetry. J Mol Recognit 2011;24(6):945–52.
[24] Fishman, J.B. and E.A. Berg, Protein A and protein G purification of antibodies. Cold Spring Harbor Protocols, 2019. 2019(1): p. pdb. prot099143 %@ 1940-3402.
[25] Phillips TM, Affinity,. *chromatography in antibody and antigen purification.* Handbook of affinity chromatography. 2nd edn. Boca Raton: CRC Press; 2005. p. 367–97.
[26] Duhamel RC et al. pH gradient elution of human IgG1, IgG2 and IgG4 from protein A-sepharose. J Immunol Methods 1979;31(3–4):211–7.
[27] Schwartz L. Immunomodulatory properties of Protein A.. San Diego, CA: Academic Press; 1990. p. 309–18.
[28] WILLIAMS, M. and T. Daviter, Protein-ligand interactions; 2016: Springer.
[29] Cantor, C.R., P.R. Schimmel, Biophysical chemistry: Part II: Techniques for the study of biological structure and function; 1980: Macmillan.
[30] Ma WN, Yang L, He LC. Overview of the detection methods for equilibrium dissociation constant K-D of drug-receptor interaction. J Pharm Anal 2018;8 (3):147–52.
[31] Hahnefeld C, Drewianka S, Herberg FW. Determination of kinetic data using surface plasmon resonance biosensors. In: Molecular diagnosis of infectious diseases. Springer; 2004. p. 299–320.
[32] Thafar M et al. Comparison Study of Computational Prediction Tools for Drug-Target Binding Affinities. Front Chem 2019;7.
[33] Mahmood MDI et al. Computational Analysis on the Binding of Epitope Peptide to Human Leukocyte Antigen Class I Molecule A*2402 Subtype. Chem Pharm Bull 2011;59(10):1254–62.
[34] Yang B et al. Molecular Docking and Molecular Dynamics (MD) Simulation of Human Anti-Complement Factor H (CFH) Antibody Ab42 and CFH Polypeptide. Int J Mol Sci 2019;20(10).
[35] Oliveira GS et al. Immobilization and unbinding investigation of the antigen - antibody complex using theoretical and experimental techniques. J Mol Graph Model 2019;86:219–27.
[36] Yannakakis MP et al. Molecular dynamics at the receptor level of immunodominant myelin oligodendrocyte glycoprotein 35–55 epitope implicated in multiple sclerosis. J Mol Graph Model 2016;68:78–86.
[37] Heymann B, Grubmuller H. Molecular dynamics force probe simulations of antibody/antigen unbinding: entropic control and nonadditivity of unbinding forces. Biophys J 2001;81(3):1295–313.
[38] Raveh B, London N, Schueler-Furman O. Sub-angstrom modeling of complexes between flexible peptides and globular proteins. Proteins 2010;78 (9):2029–40.
[39] Johansson-Akhe I, Mirabello C, Wallner B. Predicting protein-peptide interaction sites using distant protein complexes as structural templates. Sci Rep 2019;9.
[40] Kurcinski M et al. CABS-dock web server for the flexible docking of peptides to proteins without prior knowledge of the binding site. Nucleic Acids Res 2015;43(W1):W419–24.
[41] Grubmuller H, Heymann B, Tavan P. Ligand binding: Molecular mechanics calculation of the streptavidin biotin rupture force. Science 1996;271 (5251):997–9.
[42] Izrailev S et al. Molecular dynamics study of unbinding of the avidin-biotin complex. Biophys J 1997;72(4):1568–81.
[43] Isralewitz B et al. Steered molecular dynamics investigations of protein function. J Mol Graph Model 2001;19(1):13–25.
[44] Sauereriksson AE et al. Crystal-Structure of the C2 Fragment of Streptococcal Protein-G in Complex with the Fc Domain of Human-Igg. Structure 1995;3 (3):265–78.
[45] Ultsch M et al. 3-2-1: Structural insights from stepwise shrinkage of a three-helix Fc-binding domain to a single helix. Protein Eng Des Sel 2017;30 (9):619–25.
[46] Jorgensen WL et al. Comparison of Simple Potential Functions for Simulating Liquid Water. J Chem Phys 1983;79(2):926–35.
[47] Phillips JC et al. Scalable molecular dynamics on CPU and GPU architectures with NAMD. J Chem Phys 2020;153(4).
[48] Plimpton S. Fast Parallel Algorithms for Short-Range Molecular-Dynamics. J Comput Phys 1995;117(1):1–19.
[49] Huang J, MacKerell AD. CHARMM36 all-atom additive protein force field: Validation based on comparison to NMR data. J Comput Chem 2013;34 (25):2135–45.
[50] Polak, E., Ribiere, G. Note sur la convergence de méthodes de directions conjuguées. ESAIM: Mathematical Modelling and Numerical Analysis-Modélisation Mathématique et Analyse Numérique; 1969. 3(R1): p. 35-43.
[51] Hockney, R.W., Eastwood, J.W. Computer simulation using particles; 1988: crc Press.
[52] Ryckaert J-P, Ciccotti G, Berendsen HJ. Numerical integration of the cartesian equations of motion of a system with constraints: molecular dynamics of n-alkanes. J Comput Phys 1977;23(3):327–41.
[53] Andersen HC. Rattle: A "velocity" version of the shake algorithm for molecular dynamics calculations. J Comput Phys 1983;52(1):24–34.
[54] Humphrey W, Dalke A, Schulten K. VMD: Visual molecular dynamics. J Mol Graph Model 1996;14(1):33–8.
[55] Pettersen EF et al. UCSF chimera - A visualization system for exploratory research and analysis. J Comput Chem 2004;25(13):1605–12.
[56] DeLano, W.L., Pymol: An open-source molecular graphics tool. CCP4 Newsletter on protein crystallography; 2002. 40(1): p. 82-92.
[57] Zhang JL et al. Molecular Dynamics Simulations Suggest Ligand's Binding to Nicotinamidase/Pyrazinamidase. PLoS ONE 2012;7(6).
[58] Kalikka J, Akola J. Steered molecular dynamics simulations of ligand-receptor interaction in lipocalins. Eur Biophys J Biophys Lett 2011;40(2):181–94.
[59] Paci E et al. Forces and energetics of hapten-antibody dissociation: a biased molecular dynamics simulation study. J Mol Biol 2001;314(3):589–605.
[60] Kollman PA et al. Calculating structures and free energies of complex molecules: Combining molecular mechanics and continuum models. Acc Chem Res 2000;33(12):889–97.

[61] Liu, H., Hou, T. CaFE: a tool for binding affinity prediction using end-point free energy methods. Bioinformatics, 2016. 32(14): p. 2216-2218 %@ 1460-2059.
[62] Baker NA et al. Electrostatics of nanosystems: Application to microtubules and the ribosome. PNAS 2001;98(18):10037–41.
[63] Osajima, T., et al., Computational and statistical study on the molecular interaction between antigen and antibody. J Mol Graph Model; 2014. 53: p. 128-139 %@ 1093-3263.
[64] Berg, J., J. Tymoczko, Stryer, L. Biochemistry, 5th edn WH Freeman. New York. [Google Scholar]; 2002.
[65] Zacharias M. Protein-protein docking with a reduced protein model accounting for side-chain flexibility. Protein Sci 2003;12(6):1271–82.
[66] Shrake A, Rupley JA. Environment and exposure to solvent of protein atoms. *Lysozyme and insulin*. J Mol Biol 1973;79(2):351–71.
[67] Negi SS et al. InterProSurf: a web server for predicting interacting sites on protein surfaces. Bioinformatics 2007;23(24):3397–9.
[68] Sousa SF et al. Protein-Ligand Docking in the New Millennium - A Retrospective of 10 Years in the Field. Curr Med Chem 2013;20(18):2296–314.
[69] Isralewitz B, Izrailev S, Schulten K. Binding pathway of retinal to bacterio-opsin: A prediction by molecular dynamics simulations. Biophys J 1997;73 (6):2972–9.
[70] Dolinsky, T.J., et al., PDB2PQR: an automated pipeline for the setup of Poisson–Boltzmann electrostatics calculations. Nucl Acids Res, 2004. 32(suppl_2): p. W665-W667 %@ 0305-1048.
[71] Snyder PW et al. Mechanism of the hydrophobic effect in the biomolecular recognition of arylsulfonamides by carbonic anhydrase. Proc Natl Acad Sci U S A 2011;108(44):17889–94.
[72] Chandler D. Interfaces and the driving force of hydrophobic assembly. Nature 2005;437(7059):640–7.
[73] Qi PP et al. In vitro molecular evolution yields an NEIBM with a potential novel IgG binding property. Sci Rep 2014;4.
[74] Justiz-Vaillant A. Two New Immunoassays to Study the Binding Capacity of Staphylococcal Protein A (SpA) or Streptococcal Protein G (SpG) to Sera from Four Mammalian Species Including Wild and Domestic Animals. J Anal Bioanal Tech 2015;6:235.
[75] Green DVS, Leach AR, Head MS. Computer-aided molecular design under the SWOTlight. J Comput Aided Mol Des 2012;26(1):51–6.
[76] Kuhn B et al. A Real-World Perspective on Molecular Design. J Med Chem 2016;59(9):4087–102.
[77] Li RX et al. Design, synthesis, and application of a Protein A mimetic. Nat Biotechnol 1998;16(2):190–5.
[78] Currin A et al. Synthetic biology for the directed evolution of protein biocatalysts: navigating sequence space intelligently. Chem Soc Rev 2015;44 (5):1172–239.
[79] Hae Gon Lee et al. Synergistic effects of crystal structure and surface chemistry of stacked graphene-oxide membranes on the water-permeation mechanism. Desalination 2020;492(15):114603. https://doi.org/10.1016/j.desal.2020.114603. In press.